



ELSEVIER

Available online at www.sciencedirect.com

SCIENCE @ DIRECT®

Physics Letters A 311 (2003) 26–38

PHYSICS LETTERS A

www.elsevier.com/locate/pla

Characterization of the local instability in the Hénon–Heiles Hamiltonian

Juan C. Vallejo, Jacobo Aguirre, Miguel A.F. Sanjuán *

Nonlinear Dynamics and Chaos Group, Departamento de Matemáticas y Física Aplicadas y Ciencias de la Naturaleza, Universidad Rey Juan Carlos, Tulipán s/n, 28933 Móstoles, Madrid, Spain

Received 4 April 2002; received in revised form 5 February 2003; accepted 7 March 2003

Communicated by C.R. Doering

Abstract

Several prototypical distributions of finite-time Lyapunov exponents have been computed for the two-dimensional Hénon–Heiles Hamiltonian system. Different shapes are obtained for each dynamical state. Even when an evolution is observed in the morphology of the distributions for the smallest integration intervals, they can still serve for characterizing the dynamical state of the system.

© 2003 Elsevier Science B.V. All rights reserved.

PACS: 05.45.-a

1. Introduction

Lyapunov exponents are a well-known diagnostic tool for analyzing chaotic motion. In the past few years major attention has been paid in the distribution of the so-called finite-time Lyapunov exponents. As the shapes of these distributions can serve as indicators of the overall degree of instability of a system, its evolution or stationarity is a key question. Our work focuses in the study of the distributions calculated with the smallest time interval available, in order to see if they are still valid indicators, with such local information. The Letter's structure is as follows. First, we will review the different definitions found in the literature, in order to clarify many different but related

concepts. Then, a set of prototypical distributions for several orbit types in the Hénon–Heiles Hamiltonian will be shown. This conservative system has been selected, because in spite of its simplicity, it shows a large richness concerning the behavior of its orbits. Finally, we will end with some concluding remarks.

1.1. Lyapunov exponents

The ordinary (or global) Lyapunov exponent describes the evolution in time of the distance $z(t)$ between two nearly initial conditions, separated $\delta z(0)$ at $t = 0$, and it is defined in the following manner:

$$\chi = \lim_{t \rightarrow \infty} \lim_{\delta z(0) \rightarrow 0} \frac{1}{t} \log \frac{\delta z(t)}{\delta z(0)}. \quad (1)$$

Note that \log means \log_e . The global Lyapunov exponents have been proven to be a quite useful tool

* Corresponding author.

E-mail address: msanjuan@escet.urjc.es (M.A.F. Sanjuán).

for analyzing chaotic motion, and their utility comes in part from the fact that their values do not depend upon the metric. However, since in practice the calculation is performed numerically, only a finite integration time is used instead of the infinite time defined above. This leads to an approximated value instead of the real one, producing the so-called local (or finite-time) Lyapunov exponent. This is of course more important when working with experimental data, because of the very small number of measurements.

It should be noted that neither the notation nor the definitions are standard in the literature. Since this can produce some confusion, it would be worthy to summarize some of them. Some authors as in Refs. [1, 2] use the widely found terms of short-time Lyapunov characteristic numbers or local Lyapunov exponents as follows:

$$\chi(\Delta t) = \lim_{\delta z(0) \rightarrow 0} \frac{1}{\Delta t} \log \frac{\delta z(\Delta t)}{\delta z(0)}. \quad (2)$$

This quantity also appears later referred by these authors as (maximal) short-time Lyapunov exponent or finite-time Lyapunov exponent. Obviously the relation between them is

$$\chi = \lim_{\Delta t \rightarrow \infty} \chi(\Delta t). \quad (3)$$

Another widely used term is the Lyapunov characteristic number, or LCN. This is defined for instance in Ref. [3] as the limit when $t \rightarrow \infty$ of

$$\chi = \frac{1}{t} \log \frac{\delta z(t)}{\delta z(0)}. \quad (4)$$

Note that as the deviation $\delta z(0)$ is taken to be an infinitesimal, then this definition is the same that the ones in Refs. [1,2]. In addition, [4] uses the maximal LCN, as

$$\chi = \lim_{t \rightarrow \infty} \frac{1}{t} \log \frac{\delta z(t)}{\delta z(0)}, \quad (5)$$

being in essence the same that the ordinary global Lyapunov exponent.

The concept of local Lyapunov exponent (LLE) or effective Lyapunov exponent, introduced by [6–8] for studying Hamiltonian systems, appears defined in Ref. [5] as

$$\Lambda(t) = \frac{1}{t} \log \frac{\delta z(t)}{\delta z(0)}. \quad (6)$$

In this case, t can be large but finite. The algorithm for its computation will be described in the next paragraphs, since this is the definition that we have used along our study, but using the symbol $\chi(t)$ instead of $\Lambda(t)$.

The notion of stretching number, or generalized Lyapunov indicator, was introduced in [9,10], and it appears as a particular case from the local Lyapunov exponent when $t = 1$. Consequently the LCN is then the sum of stretching numbers divided by Δt . And according to [5], the average value of the stretching number is the maximal LCN.

Finally, it can be found also the term fast Lyapunov indicator, or FLI, as in [11], and the term smaller alignment index, or SALI, as in [12], as simple numerical indexes for determining if a given orbit is ordered or chaotic (see both references for detailed information).

The definition of LLE according to Eq. (6) is strongly related to the way in which the exponents are obtained. The $\delta z(t)$ is the principal semi-axis of an initial ball of radius $\delta z(0)$ after some integration steps. For the computation of the exponents, we examine the length evolution of the axes of the ellipsoid defined by a set of orthonormal D -dimensional vectors centered in the initial condition. The stretch exponents, following Refs. [13,14], are the natural logarithms of the average growth rate per iteration (also called Lyapunov number) by which the vectors expand along the D directions. The sum of the stretch exponents after N steps divided by N is the local Lyapunov exponent (or LLE) and the limit of such sum when N goes to infinity is the global Lyapunov exponent. Details concerning the computation of the Lyapunov exponents may be found in Ref. [15].

The initial orientation of the axes leads to different effective growth rates and, in consequence, following Ref. [17], the local Lyapunov exponents can be divided in two types: the finite-time Lyapunov exponents and the finite-sample Lyapunov exponents. The set of D -orthogonal vectors undergoes a few transient steps as their initial directions are chosen at random. After a few steps of integration and orthonormalization, they could be considered already locally characteristic (that means specific of a certain local flow). So the first type refers to the case when the directions coincide with the right singular vectors of the matrix resulting from the Jacobian product, and the second one,

to the case when they correspond to the vectors resulting from the evolution of those singular vectors some steps before starting the computations.

1.2. Lyapunov exponents distributions

If we make a partition of the whole integration time along one orbit into a series of time intervals of size Δt , then it is possible to compute the finite-time Lyapunov exponents $\chi(\Delta t)$ for each interval, and to plot the resulting distribution of values. By examining such spectrum, we can get information about the overall degree of instability of the orbit. Such an approach has proved to be useful in several fields such as galactic dynamics [18,19], analyzing chaotic fluid flows in the context of fast dynamos [20] or chaotic packet mixing and transport in wave systems [21]. The mean of the distribution correlates with the maximal Lyapunov characteristic number for finite sample exponents, and the shape of such distribution can serve as a valid chaoticity indicator, as it shows the range of values for χ . In principle, the shape depends on the initial condition (so on the invariant measure towards it evolves), and also on the sampling interval size Δt . The distribution of finite-time Lyapunov exponents can be normalized dividing it by the total number of intervals thus obtaining a probability density function $P(\chi)$, that gives the probability of getting a given value χ between $[\chi, \chi + d\chi]$. Hence, the probability of getting a positive $\chi(\Delta t)$ or F_+ (and analogously F_-) can be defined as

$$F_+ = \int_0^{\infty} P(\chi) d\chi. \quad (7)$$

Two ways for calculating such distributions are possible. The first one is starting from a given initial condition and integrating during the interval Δt , thus leading to a $\chi(\Delta t)$, and starting again the cycle from that point. The second way is taking an ensemble of initial conditions on the available phase space (or energy surface). For each initial point, $\chi(\Delta t)$ is calculated as before, without later progression in that orbit (see, for instance, Refs. [1,2,22]). When the phase space is largely stochastic and the regular regions small, both distributions coincide, in agreement with the ergodic theorem. If the finite intervals are large enough, the expected shapes are Gaussian, as the cen-

tral limit theorem holds and the correlations die out. However, for small finite intervals, the shapes can be different, as we will see later. In any case, when regular orbits appear, shapes can differ substantially.

1.3. Distribution behavior at very short times

We are carrying out a search on how to characterize the most chaotic orbits in a given flow. As the shapes of these distributions can serve as a valid indicator, its evolution or stationarity is a key question. This Letter follows some of the ideas started in [1,2], where the dependency on the sampling time and the evolution towards an invariant measure in the distributions from orbits in chaotic domains have been analyzed. A clear description of how these spectra characterize the dynamical state in a set of Hamiltonian prototypical cases was a motivation for our work. Many distributions belonging to typical maps have been studied, as, for instance, in [14,23,24], but less consideration has been given to conservative systems, where no attractors are found. Indeed, we are interested in the distributions for characterizing not only the possible final invariant measure, but also the orbit stability itself, including the unstable and the open orbits (those that will escape towards the infinity). The main goal will be then to generate a set of prototypical distributions for those different orbit behaviors.

Several criteria for choosing a small Δt are found in the literature. The shortest interval that can be used in the case of maps is one iteration of the map. However, for flows, as this time interval is a continuous quantity, several approaches are possible. It can be taken very small, although obviously not smaller than the integration step. It has not been completely established yet whether these finite-time Lyapunov exponents distributions are typical or stationary when computed with short intervals Δt [13].

We are interested in analyzing how the distributions calculated with the smallest available Δt interval characterize the system. Even when some variability is expected when taken such intervals, they can still serve for tracing the system. In fact, a way to determine the structure of a Lyapunov spectrum locally, that is, within some small (in principle infinitesimal) time interval is shown in Ref. [25]. Taking the interval size as small as possible, the correlation of each value

to the following one will depend only on the local orbit behavior. We will try to find out if the local information is enough for obtaining valid results or if we should increase such interval. Alternatively, the size can be equal to any time interval with physical meaning, such as the characteristic time of the system or the crossing time of the orbit with a given Poincaré section. Finally, instead of a fixed Δt , it is possible to choose a variable sampling interval, as in [4], where it is taken to be equal to the interval where the $\chi(\Delta t)$ reaches a temporary limit. On the other hand, when the size of Δt is increased, the local details are washed out. In the limit, $\chi(\Delta t \rightarrow \infty)$ tends to the global Lyapunov exponent, and the distribution tends to be a Dirac- δ centered at this global value.

2. Behavior in a two-dimensional Hamiltonian: the Hénon–Heiles system

In order to analyze distributions of finite-time Lyapunov exponents with such an approach, we have chosen the Hénon–Heiles Hamiltonian, which is a two-dimensional time independent Hamiltonian system which was originated as a model in galactic dynamics [26]. The equation of this Hamiltonian is given by

$$H = \frac{1}{2}(p_x^2 + p_y^2) + \frac{1}{2}\left(x^2 + y^2 + 2x^2y + \frac{2}{3}y^3\right). \quad (8)$$

We are interested in this model because it is connected to a physical problem and also because in spite of its simplicity it presents a rather rich complex dynamics. According to the energy of the orbit, which is related to the initial condition, different dynamic behaviors may appear and paradigmatic examples of the so-called pseudodeterministic models can be found. These models only yield to relevant information over trajectories of reasonable length due to the unstable dimension variability (see [27,28]). The oscillating behavior of the finite-time Lyapunov exponents about zero has been found to be associated to these models [24]. As we are dealing with a two-dimensional system, four Lyapunov exponents will exist. However, since it is a conservative Hamiltonian system, $\lambda_i = -\lambda_{5-i}$ for $(i = 1, \dots, 4)$ and only two different values of λ are independent. One of them will be tangent to the trajectory, parallel to the velocity field, and

the other one, transverse to it. The tangent one is non-relevant as it tends to zero in the limit case.

The distribution of the finite-time or local Lyapunov exponents was carried out by using standard methods, and the initial ellipse axes were chosen at random. We have used a sixth-order Runge–Kutta integrator with a fixed time step equal to 10^{-2} , since it provides enough accuracy for our purposes. And also we have carefully checked that the property $\lambda_i = -\lambda_{5-i}$ was kept as the integration was evolving in time, to assure the goodness of the numerical computations. The Poincaré cross-section with the plane $x = 0$ has been plotted for each state, in order to compare the distribution with the dynamical state. We have selected this plane because of the symmetry of the system with respect to it, so each orbit must repeatedly intersect it. Then, the crossing time is defined as the time between successive section crosses.

We have started the analysis computing periodic and quasiperiodic cases. In a fully stable periodic motion, as the harmonic oscillator, plotting the evolution of the $\chi(\Delta t)$ as the integration takes place, leads to plot a horizontal line, since always we get the same value $\chi(\Delta t)$ for every interval. So calculating the finite-time Lyapunov exponents distribution we get a single peaked distribution centered in a given positive value. If the interval size increases, $\chi(\Delta t \gg) \rightarrow 0$, and the peak shifts towards zero.

We can compare the former case with an orbit near an Unstable Periodic Orbit (UPO). This can be observed when the energy E takes the value $1/4$, in the Lyapunov Orbit. This orbit defines a frontier. Every orbit with an initial energy larger than the escape energy and moving outwards, if it crosses the Lyapunov Orbit, will escape from the system and will never come back (see [29]). The phase space of an example of such orbit is plotted in Fig. 1(a). For the case of an UPO, each point must avoid all regions $\chi(\Delta t) < 0$. The distribution of finite-time Lyapunov exponents is formed by two peaks, both centered around positive values. When the initial condition is slightly different from the one leading to the unstable periodic orbit, the distribution is similar to the solid line of Fig. 1(b), where we observe two broadened peaks centered around positive values, and a tail associated to the orbit once it has escaped. The two peaks are plotted when the orbit is confined, and the behavior is similar to an exact UPO. But now, the value

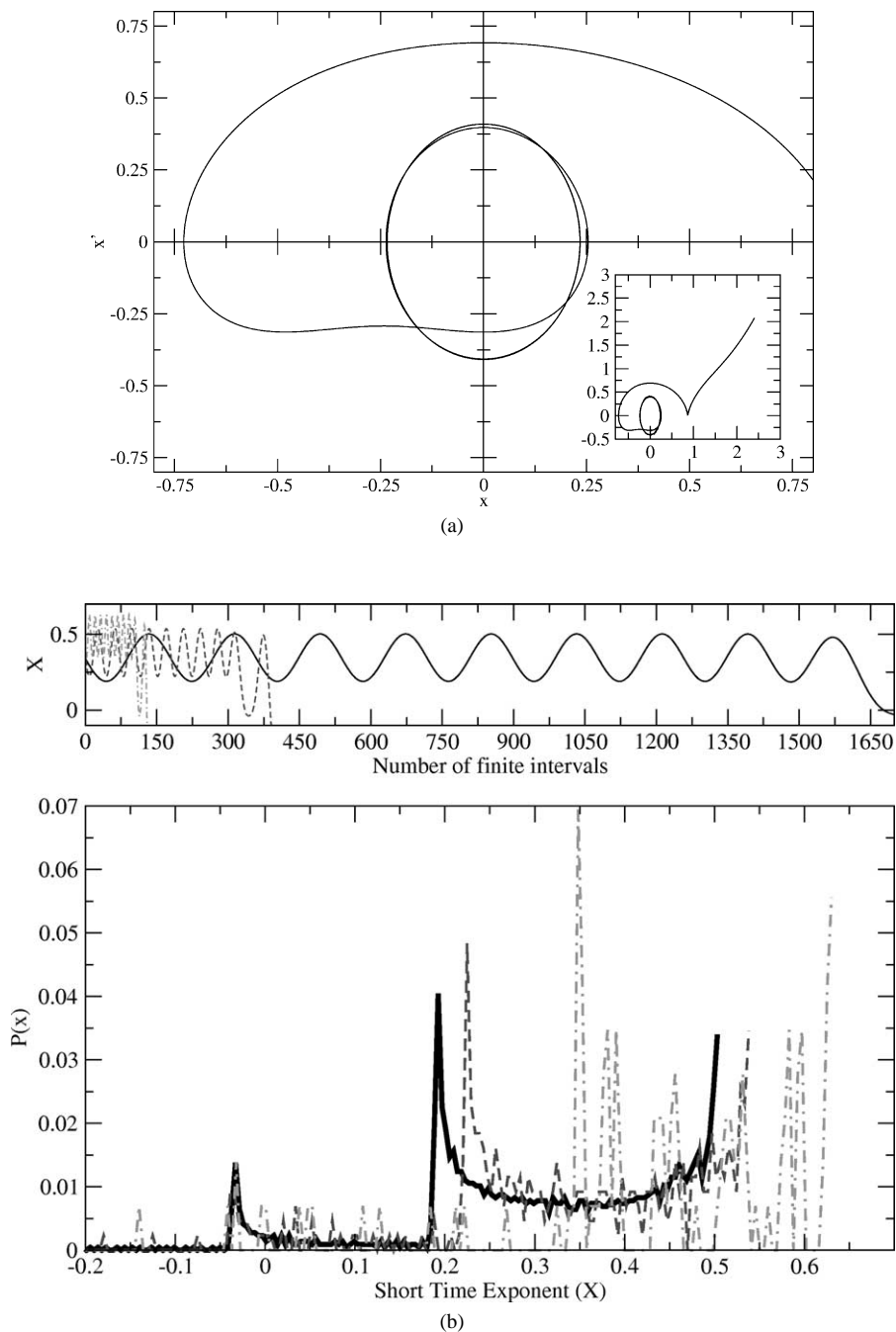


Fig. 1. (a) Orbit near an UPO, when $E = 1/4$. The period T is roughly 3.6 time-units. The figure is a zoom in of the inset which appears at the bottom right. (b) The solid line shows the probability distribution formed with an integration of 40 time-units when $\Delta t = 0.02$. The rightmost two peaks are traced when the orbit is confined, before escaping after $8T$ time-units. The dashed probability distribution is when $\Delta t = 0.1$ and the dotted one when $\Delta t = 0.3$. The smaller panel above the probability distribution figures shows the oscillating behavior of $\chi(\Delta t)$ as the integration takes place.

of $\chi(\Delta t)$ oscillates between those peaks, as shown in the solid line of the smaller panel of Fig. 1(b), leading to the intermediate spectrum of values between the main peaks.

But after having integrated $8T$ time-units, or after roughly 1600 finite intervals, the particle escapes. Now the range of values of $\chi(\Delta t)$ no longer oscillates, but get new values, leading to a left tail of totally different values, plotting, for instance, the smaller negative centered peak that appears at $t = 35$ time-units. Indeed, as shown in the smaller panel of Fig. 1(a), the motion can now follow an open track, thus the tail of the distribution extends and several small peaks centered below -0.2 (not shown) are produced. When we consider initial conditions far away from the UPO, that is orbits with smaller escape times, the general spectrum shape is different due to the tail, as it is produced by the values once the particle has escaped. But meanwhile the orbit is confined, the shape is always quite similar. If the interval size Δt is increased, but still smaller than the escaping time, it is observed that the main peaks shift towards larger positive values and begin to merge, as shown by the dashed ($\Delta t = 0.1$) and dotted ($\Delta t = 0.3$) lines of Fig. 1(b). As reflected in the smaller panel, the oscillation (around a larger value) of the finite time exponents values is preserved, but it begins to disappear after a smaller number of integrated intervals.

The following case analyzed is a quasi-periodic orbit, found in the Hénon–Heiles system for the energy $E = 1/8$. Its Poincaré surface cross section is depicted in Fig. 2(a), and it shows a set of ten islands, which is associated to a period-5 orbit. The five islands on the left are plotted when the $x = 0$ plane is crossed from the $x < 0$ subspace towards $x > 0$, and the other five on the right when returning to the $x < 0$ subspace. The distribution of finite-time Lyapunov exponents for an interval Δt of 0.02 and total integration time of 10^4 time-units is the solid line in lower panel of Fig. 2(b). It shows ten peaks, five centered around negative values and the other five centered around positive values.

In the inset panel, it has been plotted the evolution of the short time Lyapunov exponent with time (as the integrated number of intervals Δt increases). As it is a quasi-periodic orbit, it can be observed quasi-periodic oscillations, with five oscillations per larger period. These oscillations in $\chi(\Delta t)$ are shown in the

smaller inset panel. Each oscillation is associated to an island in the Poincaré section, thus to a peak in the probability distribution. Inside each period, we can count five oscillations, so five peaks are obtained in the distribution. Between each peak, a range of values is obtained, thus leading to the spectrum of values between the main peaks. As we are dealing with an orbit near a period-5 orbit, only 10 peaks can be obtained. This means that there are arbitrarily finite intervals for which the orbit, on the average, is repelling in one of the dimensions and other intervals for which is attracting in the same dimension. The shape of the distribution is independent on the initial condition along the orbit, and longer integrations (in fact, larger than 600 time-units, the circuit time or period to plot the 5 islands) do not lead to different shapes, because in this case we should only be adding more periods to the already sampled one. When the initial condition is moved far away from the periodic orbit, the distribution broadens but remains with a similar morphology.

When the interval size increases, the range of values around which the peaks are centered is reduced and it is shifted towards positive values, as shown in the lower panel of Fig. 2(b) as dotted lines, and zoomed in the upper leftmost panel. When $\Delta t = 10$, a multi-peaked probability distribution is still observed, since this value is larger than the crossing time but still smaller than the total circuit time, which is roughly 32 time-units. This case is found as dashed-dotted in the upper rightmost panel. For larger sizes of time intervals the peaks begin to merge, as Δt begins to be equal to the circuit time.

This behavior is different for orbits showing some chaoticity. One example appears in Fig. 3(a), with initial energy $E = 1/12$. The solid line in Fig. 3(b) shows the corresponding probability distribution with an integration time of 20 000 units, and $\Delta t = 0.02$. The whole available phase space is traced and longer integrations lead basically to the same shape. This shape does not correspond to a “typical” chaotic state, where the central limit theorem holds for a number of averaged quantities, including local Lyapunov exponents (see [8,16]) and the distributions can be fitted by a Gaussian, since the correlations die out. Neither does it to an intermittent system, where the shape might be a combination of a normal density and a stretched exponential tail, due to the long correlation persistence.

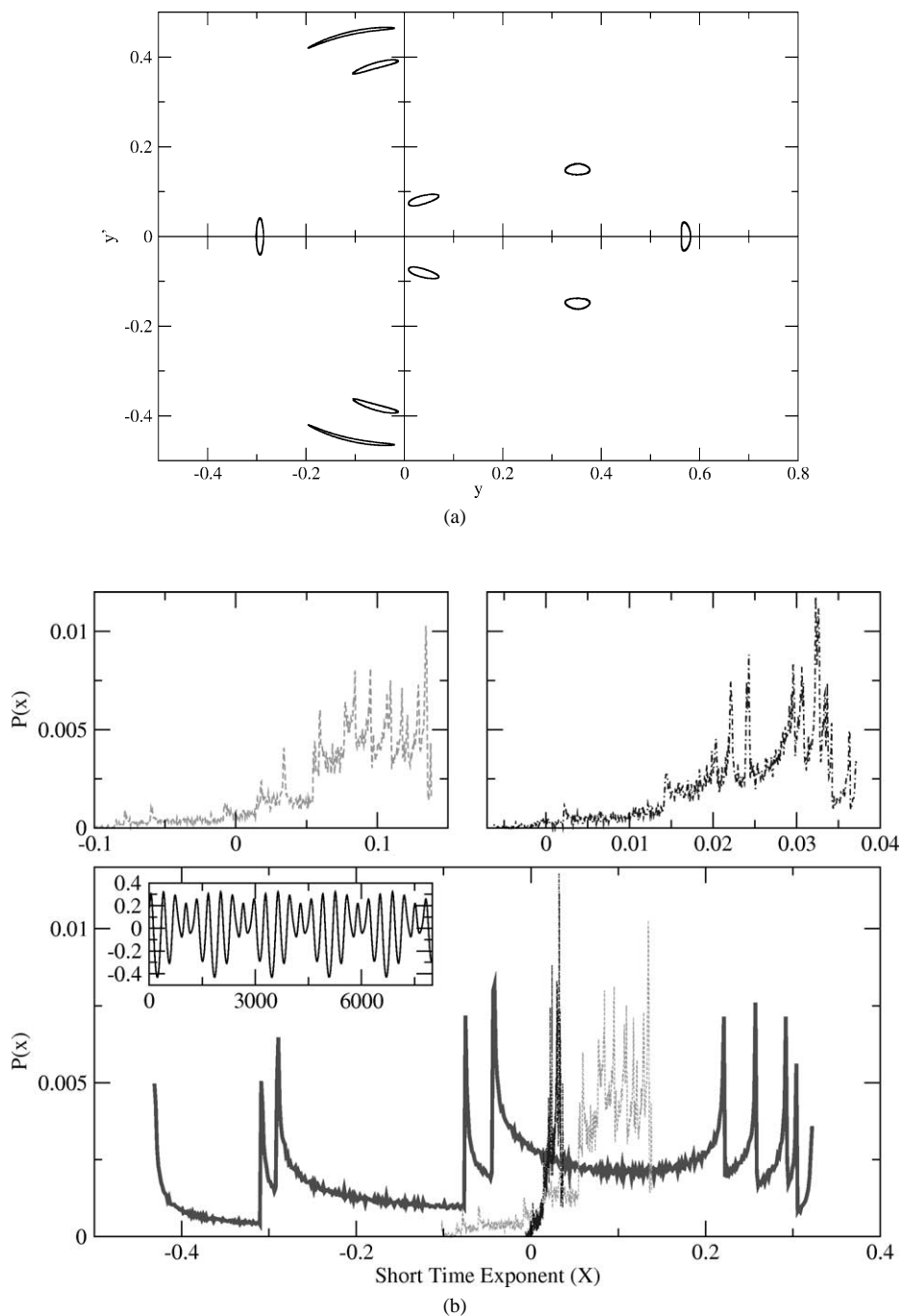


Fig. 2. (a) Poincaré cross-section of a quasi-periodic orbit of energy $E = 1/8$, associated to a period-5 orbit. The crossing time is approximately 6.2 time-units. Each time a point crosses the section, a different island is crossed and the total time before repeating an island is roughly 31.5 time-units. (b) The lower and larger panel shows the probability distribution of finite-time Lyapunov exponents, showing 10 peaks both in positive and negative values, when $\Delta t = 0.02$ and total integration time 10^4 time-units. The dashed probability distribution is when $\Delta t = 10$ and integration time 10^6 , and is zoomed in the upper leftmost panel. The dotted line represents the probability distribution when $\Delta t = 100$ and integration time 10^6 , and is zoomed in the upper rightmost panel.

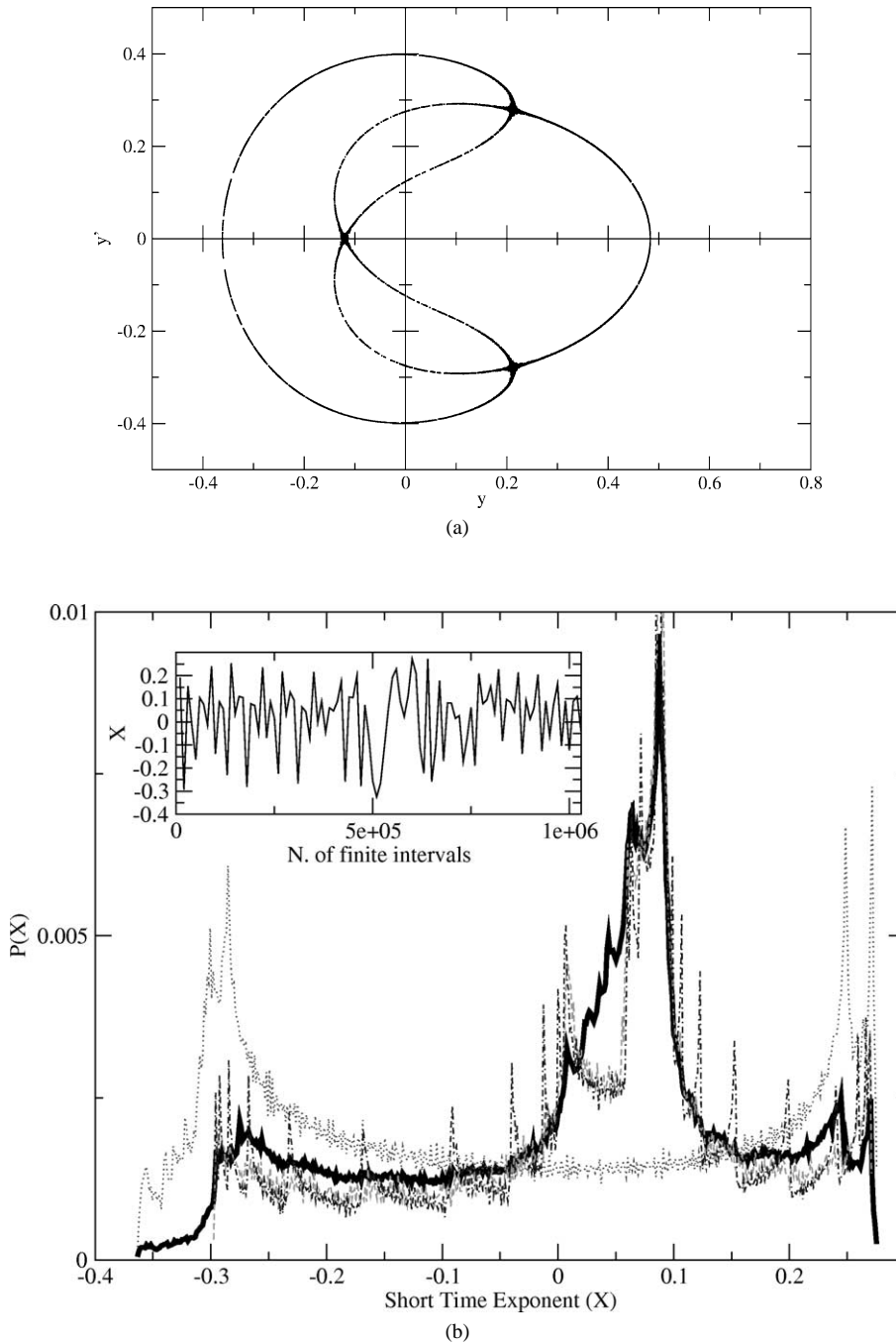


Fig. 3. (a) Poincaré cross-section of an orbit of energy $E = 1/12$. The crossing time is approximately 6.75 time-units. (b) The solid line shows the probability distribution of finite-time Lyapunov exponents formed with an integration of 20 000 time-units when $\Delta t = 0.02$. The dotted and dashed lines represent the probability distributions corresponding to partial 1000 time-units integrations started at arbitrary points of the same orbit. These partial integrations reflects some of the different transients of Table 1. The smaller panel shows the oscillating behavior of $\chi(\Delta t)$ as the integration takes place.

As we are analyzing the evolution or stationarity of the probability distributions, it is important to keep in mind the difference between stationarity, due to the dynamics at certain time, and ergodicity, time-averaged property of the trajectories. In a non-ergodic orbit, the trajectory does not cover the whole hypersurface of constant energy, so two different initial conditions cover different parts of the energy surface leading to different temporal averages even for times tending to infinity. In such systems there is not a unique equilibrium state, but different ones depending on the starting point. Conversely, a unique equilibrium state can be reached in an ergodic. And generic ensembles of initial conditions will evolve towards a given distribution, time-independent or with little variability on long time-scales. One key point is the time involved in such evolution towards the final state. If the physical time scales are relevant and that time is too long for being realistic, those ensembles will not be able to be used as a valid skeleton for the observed system behavior.

So when computing probability distributions from a set of initial conditions, we need to be sure that they are in the same domain of the Poincaré section. In that case, we get again the solid histogram of Fig. 3(b). On the other hand, the stationarity of a distribution can be defined when the statistical parameters do not change with time, and this depends on the variable dynamics along the given orbit. When the probability distribution from a single orbit is computed, the morphology may depend on the initial point, when the total integration time is not large enough, as several transients of different behavior are found (see Ref. [17]).

In order to catch the behavior of the transient periods, we have computed probability distributions formed integrating just 10^3 time-units (150-times the crossing time), which are described in Table 1.

Three of them appear in Fig. 3(b). The characteristic time on which the orbit forgets its previous degree of instability is small (low correlation time), as they are quite different. The standard deviation of the distributions σ gives a measure of the degree in which χ deviates from the mean, being a measure of the stability or variability of the values of χ along the orbit. The probability of getting a positive value for a finite-time Lyapunov exponent F_+ takes different values ranging from 0.4 up to 0.7 quite randomly, what indicates

Table 1

Several probability distribution behaviors in the case $E = 1/12$ for the smallest interval size $\Delta t = 0.02$. The statistics are for integrations of 10^3 time-units starting at t_0

t_0	Mean	Std. Dev.	Median	$F_+(t_0)$
0	-0.04402	0.18489	-0.44017	0.43455
10^3	-0.01337	0.16457	-0.01337	0.67674
2×10^3	-0.01318	0.16437	-0.01318	0.66708
3×10^3	-0.01318	0.16438	-0.01318	0.67882
12×10^3	-0.04406	0.18492	-0.04406	0.47806
14×10^3	-0.016346	0.152195	-0.016346	0.700080

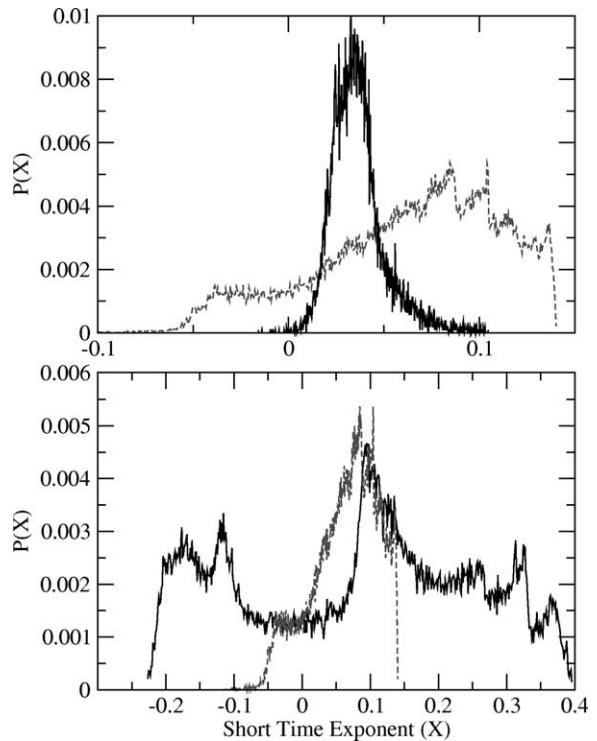


Fig. 4. The distribution of finite-time Lyapunov exponents in the case $E = 1/12$ formed with an integration of 10^6 time-units when $\Delta t = 1$ is plotted as solid line in the lower panel. The same when $\Delta t = 10$ appears in dashed line, and is zoomed in the upper panel. In this later one, it is also traced the distribution when $\Delta t = 100$.

different behaviors, regular at some stages, chaotic in others, as reflected in the shape of the distributions. For instance, the first transient shows two well separated peaks, like a quasi-periodic orbit (dotted line), while the third transient shows a multi-peaked distribution (dotted-dashed line). When the time evolution of the finite-time Lyapunov distributions (and the

Table 2

Several distribution behaviors in the case $E = 1/12$ for interval size $\Delta t = 1$. The statistics are for integrations of 10^3 time-units starting at t_0

t_0	Mean	Std. Dev.	Median	$F_+(t_0)$
0	0.07362	0.17391	0.07362	0.46000
10^3	0.09552	0.17119	0.09552	0.74000
2×10^3	0.09293	0.17478	0.09293	0.72000
3×10^3	0.09117	0.17415	0.09117	0.73000
12×10^3	0.06484	0.16613	0.06484	0.51000
14×10^3	0.08573	0.14284	0.08573	0.75000

time evolution of $\chi(\Delta t)$ itself, as shown in the smaller panel) is compared with the way the consequents of the Poincaré section fill the available phase space, we see how each distribution corresponds to a different way of tracing the Poincaré section.

If we change the interval size Δt by a small integer factor, our result is only a rescaling of the spectrum, as was shown in Ref. [19]. However, when it is increased up to, say, $\Delta t = 1$, which is still smaller than the averaged crossing time, a different multi-peaked shape is obtained, as the solid line in the lower panel of Fig. 4 shows. The local details are washed up as the interval size is larger than the crossing time, so with a $\Delta t = 10$ (dotted line), the shape is again different. This distribution is zoomed in the upper panel and two smooth peaks well fitted by Gaussians, the main one centered around positive values are observed. For even larger values of $\Delta t = 100$, a probability distribution with a the form of a single peak Gaussian is found, which is plotted as a solid line in the upper panel of Fig. 4, since the central limit theorem begins to hold. Finally, for much larger values of $\Delta t = 100$, the distributions collapse to δ -functions centered around the global Lyapunov value. In addition, the chaoticity indicators vary with the interval size. The values in Table 2 are calculated as in Table 1, so here it appears

the statistics for the transients with an integration (sampling) of $\Delta t = 1$.

The mean value calculated with the larger interval on each transient is different to the calculated one with the smallest interval. Moreover, the values of F_+ are larger, and for even larger interval sizes, the transients may vanish. Nevertheless it is remarkable that the evolution of F_+ , which is an indicator of the local chaoticity, is similar in both cases. The Table 3 shows how the total integration time for a given interval size is correlated with these indicators, showing that for the smallest interval we obtain similar results.

This can be explained indicating that by integrating 2×10^4 time-units, we have already passed through all possible values of the oscillating short time Lyapunov exponent, so even increasing the total integration time up to 2×10^5 time-units, the spectrum is basically the same. For larger intervals, the statistics is poorer, as the total number of intervals taken into account is smaller, but the same reasoning can be used. When $\Delta t = 1$, we are still getting almost the same pattern in the oscillations with 2×10^4 time-units or 2×10^5 , so the values are still quite similar. But with $\Delta t = 10$, the values are slightly different, as the pattern of the oscillations of the short time Lyapunov exponent is also slightly different.

Finally, the characterization of the distributions corresponding to chaotic orbits is discussed. We take an orbit with an initial energy $E = 1/8$, that almost fills completely the available phase space, as shown by the Poincaré cross section in Fig. 5(a). The corresponding probability distribution is plotted as a solid line in Fig. 5(b). The smaller panel shows again the oscillations of $\chi(\Delta t)$ as the integration takes place. The same probability distribution is obtained by integrating along a single initial condition or an ensemble of initial conditions, due to the ergodicity of the system. The shape reminds the one described for attractors in

Table 3

Sensitivity of the statistics of the finite-time Lyapunov distributions in the case $E = 1/12$ for several integration time and interval sizes

t (total time)	Δt (time)	Mean	Std. Dev.	Median	$F_+(t_0)$
2×10^4	0.02	-0.04403	0.18490	-0.04403	0.64226
2×10^5	0.02	-0.04407	0.18492	-0.04407	0.65772
2×10^4	1	0.08553	0.17873	0.08553	0.69000
2×10^5	1	0.08454	0.18004	0.08454	0.71060
2×10^4	10	0.03215	0.06258	0.03215	0.90400
2×10^5	10	0.02509	0.06671	0.02511	0.89565

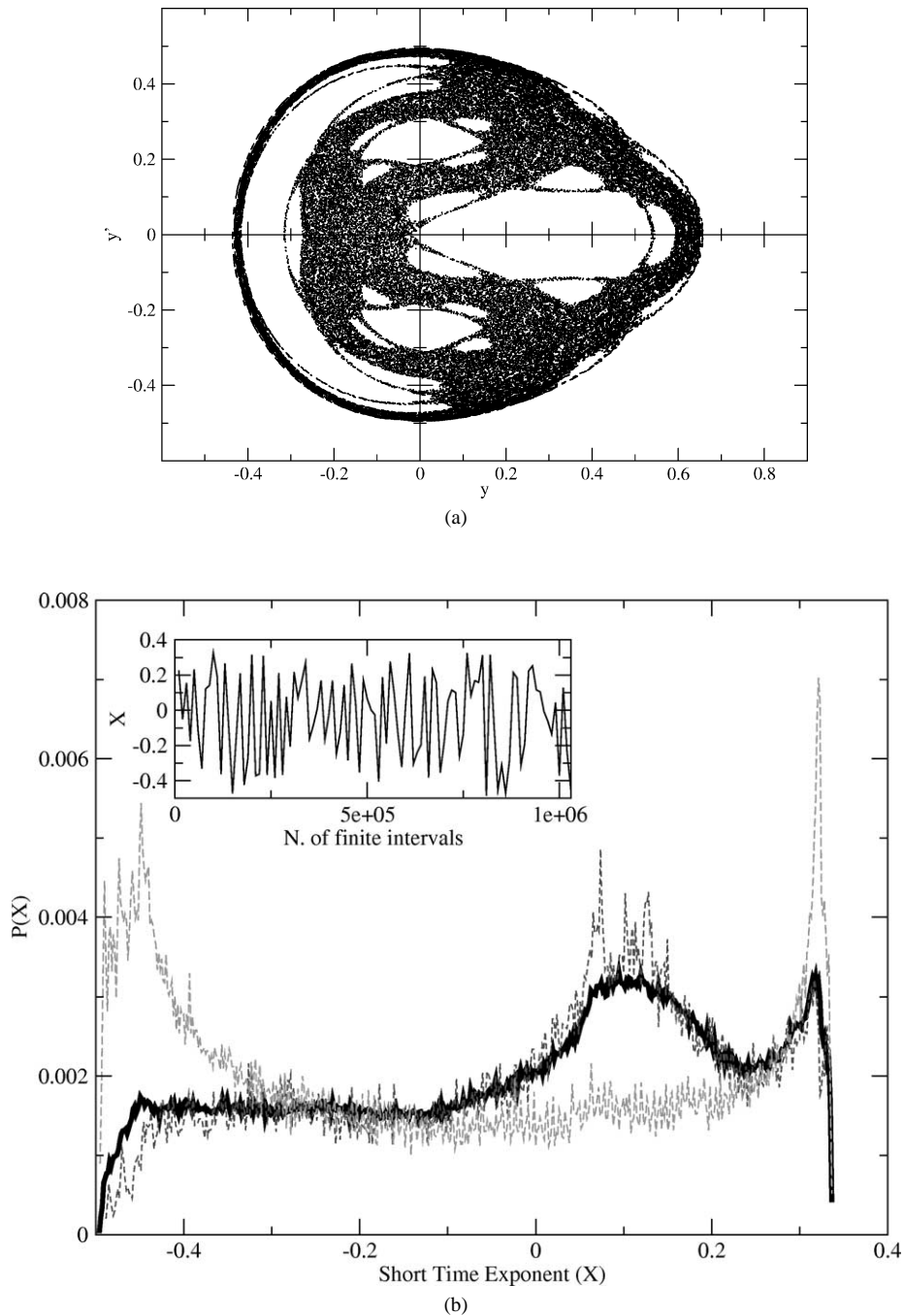


Fig. 5. (a) Poincaré cross-section of an orbit of energy $E = 1/8$. The crossing time is approximately 6.80 time-units. (b) Probability distribution of finite-time Lyapunov exponents. The solid line corresponds to an integration of 20000 time-units when $\Delta t = 0.02$. The dotted and dashed ones to partial integrations of 10^3 time-units. The double peaked one corresponds to a sticky period. The smaller panel shows the oscillating behavior of $\chi(\Delta t)$ as the integration takes place.

Refs. [23,28], although the tail of the peak centered around positive values extends through negative values quite smoothly, instead of showing an exponential tail. Two different transients of 10^3 time-units are plotted as dotted and dashed lines in Fig. 5(b). We also see that the sticky orbits, those that remain near a regular island for a long time, tend to have smaller exponents than the non-sticky orbits. During the sticky periods, when the orbit appears next to a quasi-periodic orbit torus, the distribution is clearly similar to a quasi-periodic case. However, in the chaotic regime the peaks are broadened. With larger intervals ($\Delta t = 10$) and integration times (10^6 time-units), an almost Gaussian shaped distribution is obtained, centered around a positive value. This shows a morphology different from the $E = 1/12$ case, that did not reach such Gaussian form even when $\Delta t = 10$, meaning a different dynamics, which is also manifested by the time the distribution takes to its final state.

Such different morphology can be seen by comparing the solid lines of Fig. 3(b) and Fig. 5(b). In the later case, the peak is not so clear, and the distribution is smoother, indicating that there is no larger probability of getting a value over another one. In the previous case, there is a clear peak, indicating that there is a high probability of getting the range of values on which the peak is constructed. So the later case indicates that there is more “chaoticity” in the sense that there are no privileged values, as in the $E = 1/12$ case, so there is a larger ergodicity, in the sense that the orbit is able to reach with the same probability all the available phase space. However, it should be taken into account that during certain transient periods, the behavior is equivalent to regular motions, as during the sticky transients (double-peaked distributions).

3. Conclusions

The results presented here are of general interest in describing how the distributions of finite-time Lyapunov exponents are valid indicators when computed with the smallest time interval. Several prototypical distribution morphologies have been plotted for different energy values of the Hénon–Heiles Hamiltonian. These calculations can be carried out in three ways. First, calculating a huge number N of short-time exponents of size Δt along the same orbit. Second, tak-

ing a smaller number of larger Δt (to allow the values to saturate). Third, selecting carefully an ensemble of N initial conditions in the same domain.

Our calculations have focused in the use of the smallest interval size, searching for the stationarity or evolution of the distributions. It has been observed that they characterize the motion in the different possible cases. Shapes well differentiated from the ones described in the literature have been found as they depend both on the motion type, the interval size and the integration time. In the fully regular motion, the shape is independent on the size of the chosen small interval. When the case of a UPO was analyzed, it was observed the importance of the size of the interval with respect to the time the particle was confined before escaping. In the quasi-periodic case, the final shape is independent of the initial point along the orbit and is reached after a small integration time (a few times the crossing time). For larger intervals, the shape is still well differentiated from the other cases, even when a short integration time is used. In the chaotic motions of energy values $E = 1/12$ and $E = 1/8$, the shape depends strongly on the initial point for short total integration times, since the distribution evolves through several transients and consequently several cycles are required before reaching the final shape. According to Ref. [5], the spectrum of chaotic orbits is invariant with respect to the initial conditions along the same invariant curve, but this only is applicable for large integrations or large intervals. However, tracing the distributions with the smallest intervals gives information on the local evolution of the stability for short time scales. The morphology of the distributions traces the dynamics and the evolution of the value F_+ is the same independently of the interval size.

One interesting point is to analyze the sources of the components of the distribution morphology. The local behavior is given by the local exponents, thus the overall shape depends on the local orbit behavior, as the exponents can be considered specific of a certain local flow. And as we have seen, the overall behavior is the sum of the different behaviors: the ones corresponding to the smaller intervals when the local exponents were calculated. In addition, the local orbit behavior can be understood in terms of simpler periodic orbits, as possible basic blocks for shadowing the observed complicated behavior. This is a quite interesting research topic that can extend the current

results, by studying the role of such periodic orbits in the construction of the structures described here.

As different parts of the same chaotic orbit may show different local exponents values in the different transients, this would indicate that the chaotic phase mixing [30] could be larger than the regular phase mixing at certain physical relevant time scales. We may conclude from here that different rates might exist in the evolution of the system towards its final state.

Our analysis has focused in a Hamiltonian system, where the stochastic orbits are ergodic. In this case, the results from generating the distributions from an adequate ensemble or from a single orbit are equivalent. But by taking the later approach, we were also able to manage with the distributions of non-ergodic orbits. The results obtained with this approach should be valid for orbits both in conservative or non-conservative systems, and in the case of dissipative systems, the distributions of the attractors described in the literature can be found. But as an evolution towards a final distribution is not guaranteed in a given time, the results on the stationarity or evolution during that period hold.

In addition, for two-dimensional Hamiltonians as this one, the existence of KAM tori produces the existence of sticky and non-sticky orbits, so the described phenomenology on the sticky transients is specific of this type of systems. It should be remarked that for three-dimensional Hamiltonians, the cantori appear and this is no longer applicable since, in the end, the Arnold diffusion produces a merging of the orbits.

The previous discussion shows also some implications from the physical meaning of the system. As the long integrations required for computing the global Lyapunov exponents have no meaning in a galactic system, since the universe evolves in a shorter time, it is reasonable to use smaller integrations. Furthermore, the smallest interval sizes can be used since they characterize the local behavior.

Acknowledgements

We would like to thank Prof. Juergen Kurths for the critical reading of this manuscript, his fruitful comments and some discussions. The computations of the orbits have been performed with the software DYNAMICS [31]. This work has been supported by the Spanish Ministry of Science and Technology under

project BFM2000-0967, and by the Universidad Rey Juan Carlos under projects URJC-PGRAL-2001/02 and URJC-PIGE-02-04.

References

- [1] H.E. Kandrup, M.E. Mahon, *Astron. Astrophys.* 290 (1994) 762.
- [2] M.E. Mahon, R.A. Abernathy, B.O. Bradley, H.E. Kandrup, *Mon. Not. R. Astron. Soc.* 275 (1995) 443.
- [3] G. Contopoulos, N. Voglis, *Astron. Astrophys.* 317 (1997) 73.
- [4] K. Tsiganis, A. Anastasiadis, H. Varvoglis, *Chaos Solitons Fractals* 11 (2000) 2281.
- [5] G. Contopoulos, E. Grousosakou, N. Voglis, *Astron. Astrophys.* 304 (1995) 374.
- [6] H. Fujisaka, *Prog. Theor. Phys.* 70 (1983) 1264.
- [7] R. Benzi, G. Parisi, A. Vulpiani, *J. Phys. A* 18 (1985) 2157.
- [8] P. Grassberger, R. Badii, A. Politi, *J. Stat. Phys.* 51 (1988) 135.
- [9] C. Froeschlé, Ch. Froeschlé, E. Lohinger, *Celestial Mech. Dynam. Astron.* 56 (1993) 307.
- [10] N. Voglis, G. Contopoulos, *J. Phys. A* 27 (1994) 4899.
- [11] C. Froeschlé, X. Lega, X. Gonczi, *Celestial Mech. Dynam. Astron.* 67 (1997) 41.
- [12] X. Skokos, *J. Phys. A* 34 (2001) 10029.
- [13] A. Prasad, R. Ramaswamy, *Phys. Rev. E* 60 (1999) 2761.
- [14] F.K. Diakonou, D. Pingel, P. Schmelcher, *Phys. Rev. E* 62 (2000) 4413.
- [15] K. Alligood, T.D. Sauer, J.A. Yorke, *Chaos. An Introduction to Dynamical Systems*, Springer-Verlag, New York, 1996, p. 383.
- [16] E. Ott, *Chaos in Dynamical Systems*, 2nd Edition, Cambridge Univ. Press, 2002.
- [17] C. Ziehmann, L.A. Smith, J. Kurths, *Phys. Lett. A* 271 (2000) 237.
- [18] P.A. Patsis, C. Efthymiopoulos, G. Contopoulos, N. Voglis, *Astron. Astrophys.* 326 (1997) 493.
- [19] H. Smith, G. Contopoulos, *Astron. Astrophys.* 314 (1996) 795.
- [20] J.M. Finn, J.D. Hanson, I. Kan, E. Ott, *Phys. Fluids B* 3 (1991) 1250.
- [21] H. Yang, *Int. J. Bifurc. Chaos* 3 (1993) 1013.
- [22] C. Siopis, H.E. Kandrup, G. Contopoulos, R. Dvorak, *Celestial Mech. Dynam. Astron.* 65 (1997) 57.
- [23] A. Prasad, R. Ramaswamy, Finite-time Lyapunov exponents of strange nonchaotic attractors, in: M. Daniel, R. Sahadevan, K. Tamizhmani (Eds.), *Nonlinear Dynamics: Integrability and Chaos*, Narosa, New Delhi, 2000, p. 227.
- [24] R.L. Viana, C. Grebogi, *Phys. Rev. E* 62 (2000) 462.
- [25] H.R. Moser, P.F. Meier, *Phys. Lett. A* 263 (1999) 167.
- [26] M. Hénon, C. Heiles, *Astron. J.* 69 (1964) 73.
- [27] Y.-C. Lai, C. Grebogi, J. Kurths, *Phys. Rev. E* 59 (1999) 2907.
- [28] E.J. Kostelich, I. Kan, C. Grebogi, E. Ott, J.A. Yorke, *Physica D* 109 (1997) 81.
- [29] J. Aguirre, J.C. Vallejo, M.A.F. Sanjuán, *Phys. Rev. E* 64 (2001) 066208.
- [30] H.E. Kandrup, *Mon. Not. R. Astron. Soc.* 301 (1998) 960.
- [31] H.E. Nusse, J.A. Yorke, *Dynamics: Numerical Explorations*, 2nd Edition, Springer, New York, 1998.